Electronic Supplementary Material (ESI) for Materials Horizons.

Supporting Information for

Self-association and gel formation during sedimentation of like-charged colloids

Xufeng Xu, Gijsbertus de With* and Helmut Cölfen*

Table of Contents

List of important symbols:

z: surface charge number
e: charge on a single electron
ε_0: electric permittivity of vacuum
ε_r: electric permittivity of solvent
ξ: zeta potential
R: particle radius
κ^{-1}: Debye length
s: sedimentation coefficient
D_t: translational diffusion coefficient
M: particle molecular mass
$\bar{\nu}$: partial specific volume
ρ_s: solvent density
RT: product of the molar gas constant R and the temperature T
kT: product of the Boltzmann constant k and the temperature T
r: radial position, which indicates the radial distance from the center of rotation
r_m: radial position of meniscus
ρ: particle number density
m: particle mass
ω: angular velocity of centrifugation
y: non-dimensional number density
L_ω: gravitational length
c: mass concentration
c_m: mass concentration at meniscus
c_s: ion concentration
B_2 and B_3: second and third virial coefficient, respectively
a: activity
f: activity coefficient
$\Delta\Pi$: osmotic pressure difference
$\Delta\mu$: chemical potential difference
ε_1 and ε_2: dielectric constant of solvents and nanoparticles, respectively
n_1 and n_2: refractive index of solvents and nanoparticles, respectively
H: interparticle distance
A: Hamaker constant
Ψ_0: surface potential
ν_e: plasma frequency of the free electron gas
h: Planck constant
U_A and U_R: vdW attraction force potential and electrostatic repulsion force potential, respectively
l_B: Bjerrum length
b: charge site spacing

Experimental Procedures

1) Synthesis of fluorescein/rhodamine labeled silica nanoparticles

Fluorescein/rhodamine labeled silica nanoparticles (diameter = 84 nm, PDI = 0.09) were regrown from 30 nm fluorescence labeled silica core particles[1]. 80 mg arginine, 22.5 mL water, 90 mL ethanol, 1.8 mL core dispersion and 0.55 g tetraethyl orthosilicate (TEOS) were added to a clean 250 mL glass reaction vessel. The reaction was carried out at 70 °C with stirring for 5 hours. Thereafter, 0.55 g TEOS was added and the reaction was continued overnight. The size of the synthesized silica nanoparticles was characterized by scanning electron microscopy (SEM) (as shown in **Figure S13**). The synthesized nanoparticles were purified by dialysis or repeated centrifugation until a constant conductivity was reached.

We note that the size for Stöber silica as measured by SEM is often smaller than as measured by DLS or sedimentation, an effect often attributed to further condensation under the influence of the electron beam. As here arginine was used as a base source, it is not right away clear whether shrinkage for such particles in SEM also occurs. Moreover, although often size measured by DLS shows a somewhat larger value than as measured by microscopy[2], this is not always the case[3]. Generally, a comparison of the results of these methods is not straightforward at all[4–6].

2) Analytical ultracentrifugation experimental details

In a typical sedimentation-diffusion equilibrium (AUC-SE) experiment, a home-made multi-wavelength analytical ultracentrifuge [7,8](MWL-AUC) with AUC titanium double sector cells of 1.5 mm pathlength (Nanolytics GmbH, Potsdam, Germany) was used. An appropriate amount (10 ~ 20 μL) of the sample was added into the sample cell by a syringe and slightly more 80% glycerol was added into the reference cell. With the thus prepared cell MWL-AUC experiments were done at 25 °C using the wavelength range 250 – 700 nm (spectrometer resolutions 1 nm) and radial steps of 1 or 2 μm with scan intervals of 3600 s. Typically, sedimentation-diffusion equilibrium was reached after 7 days, as checked by an unchanged concentration gradient for 10 h. The resulting datasets were processed by the home-developed software MWL-Viewer. Concentration-radial position curves, such as in **Figure 2**, were fitted using the Origin software.

3) Electrophoretic experiment

The ion concentration for the silica dispersion (3×10^{22} /m^3 assuming that monovalent H^+ and OH^- ions were present) was estimated from the electrical conductivity (1.0 μs/cm), as measured using a conductivity meter (Schott Instruments, Lab 960). The zeta potential was measured by a Malvern Zetasizer Nano ZSP. The conversion from electrophoretic mobility to zeta potential was achieved by using the Henry equation. The Smoluchowski approximation was used because it is suitable for samples suspended in aqueous solutions. The colloidal concertation used was very diluted. The solvent composition used was 65 vol% glycerol + 35 vol% water. When the volume fraction of glycerol increased above 65%, the signal became extremely weak due to nearly refractive index matching. Therefore, the zeta potential at 65 vol% glycerol was the best approximation for the zeta potential at the refractive index matching composite of 80 vol% glycerol. The evolution of zeta potential as a function of glycerol composition is shown in **Figure S14**. The surface charge number z was finally estimated using the Debye-Hückel approximation[9]: $ze = 4\pi\varepsilon_0\varepsilon_r|\xi|R(1+R\kappa)$ where ε_0 and ε_r are the electric permittivities of vacuum and solvent respectively, ξ is zeta potential, R is the particle radius and κ^{-1} is the Debye length.

SI 1: The analysis of oligomer peaks from sedimentation velocity (AUC-SV) experiment

The sedimentation coefficients s of oligomers can be calculated from the s value of monomers (the term 'oligomers' and 'monomers' are used as a jargon analogous to their use in polymer science) by using the translational diffusion coefficient D_t ratio of oligomers over monomers[10] (**Table S1**) and applying the Svedberg equation (S1)

$$s/D_t = M(1-\bar{\nu}\rho_s)/RT \qquad \text{(S1)}$$

with M the particle molecular mass, $\bar{\nu}$ the partial specific volume of particles and ρ_s the solvent density. Since the molecular mass ratios of oligomers and monomers are known, the specific volume of the particles and the solvent density are fixed the sedimentation coefficients s of oligomers can be calculated from the s value of the monomer using the normalized translational diffusion coefficient D_t. **Table S1** provides an example for the clusters of 2 and 3 particles, also showing the calculation results and a comparison with the experimental data. Excellent agreement was obtained and all the peaks can be recognized in **Figure S1a.** This figure shows that the dispersion consists of monomers, various kinds of oligomers and also that larger clusters with more complicated configurations are present. These oligomers were introduced in a reproducible way by the synthesis protocol described in **Experimental Procedures** section.

Oligomer	Monomer	Dimer	Trimer (triangle)	Trimer (linear)	Larger cluster
Normalized D_t	1	0.75	0.66	0.60	…
s_{theo} (S)	53	79	105	95	…
s_{exp} (S)	53	78	105	93	…
Deviation (%)	0	1	0	2	…

Table S1: Normalized translational diffusion coefficients D_t of the various oligomers, such as dimers and trimers (*10*) and the theoretical (s_{theo}) and experimental (s_{exp}) sedimentation coefficients of different oligomers, such as dimers and trimers.

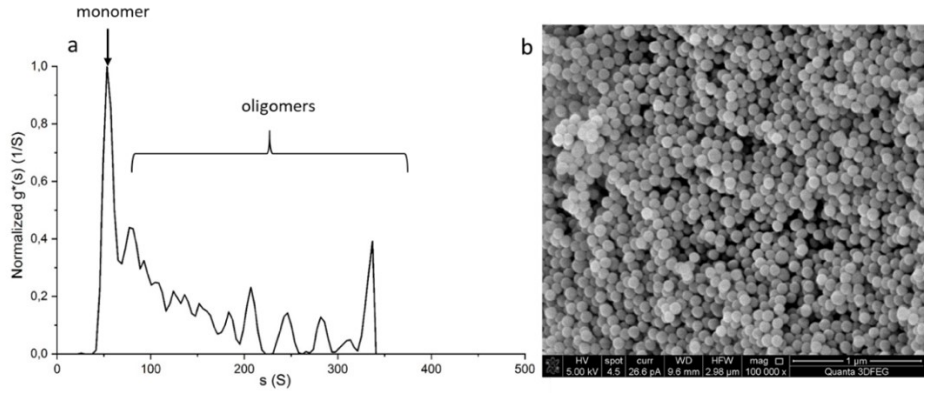

Figure S1: a) Distribution of the sedimentation coefficient *s* of SNPs in dispersion, measured by an AUC sedimentation velocity (AUC-SV) experiment using the *g**(*s*) model with the software Sedfit (*11*); b) A representative SEM image of the synthesized SNPs after drying.

In comparison, a reverse micro-emulsion method[12] and a subsequent seeded Stöber method[13] were used for monodisperse, fluorescent-labeled silica nanoparticle synthesis with a final size of ca. 100 nm (as shown in **Figure S2a**). The detailed synthesis route is as follows: Fluorescein/rhodamine labelled silica nanoparticles were regrown from 60 nm fluorescent labelled silica core particles. Of the silica core dispersion 3 mL (6.7 mg mL^{-1}) was diluted with 1.5 mL 25% ammonia and 15.5 mL ethanol in a clean 50 mL glass reaction vessel. A mixture of 0.28 mL tetraethyl orthosilicate (TEOS) and 0.56 mL ethanol was then added. The reaction was carried out at room temperature with stirring at 800 rpm for overnight and resulted in particles of 100 nm. The surface charge number of these nanoparticles was ca. 130. As can be seen in **Figure S2b**, the concentration gradient formed in this case can only rise until ca. 40 vol% and *region III* is missing, as compared to **Figure 1**.

The presence of oligomers induced an environment with a degree of crowding, which for a monodisperse dispersion is hardly reached**.** Without any oligomer, the highest volume fraction only reached ca. 40 vol%, while with the presence of oligomers the particle concentration can reach 60 vol%. Therefore, the interparticle distance becomes smaller and this high-density region is labeled as an environment of super-crowding, due to which *region III* was formed.

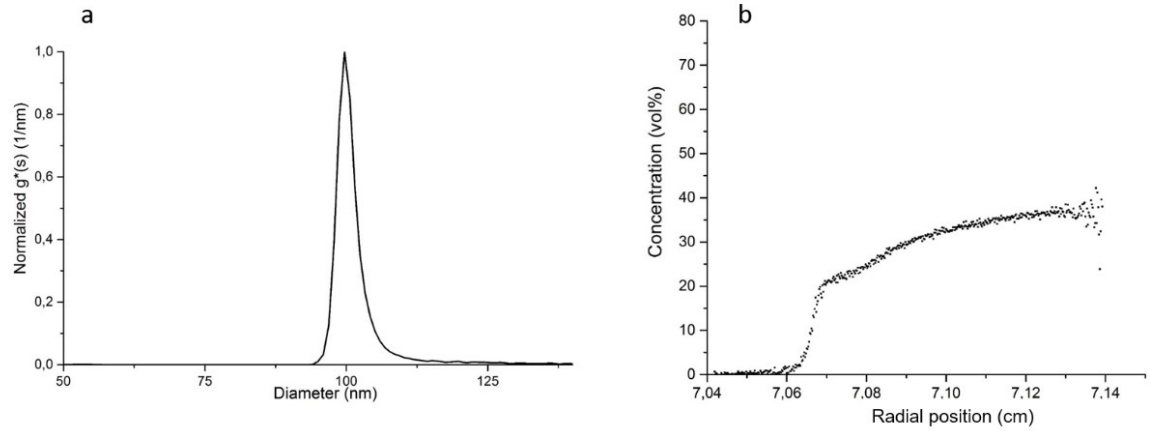

Figure S2: a) Size distribution by AUC-SV and b) Experimental sedimentation-diffusion equilibrium concentration profiles for the concentrated charged SNP suspensions at an initial concentration of ca. 15 vol% at 1100 rpm.

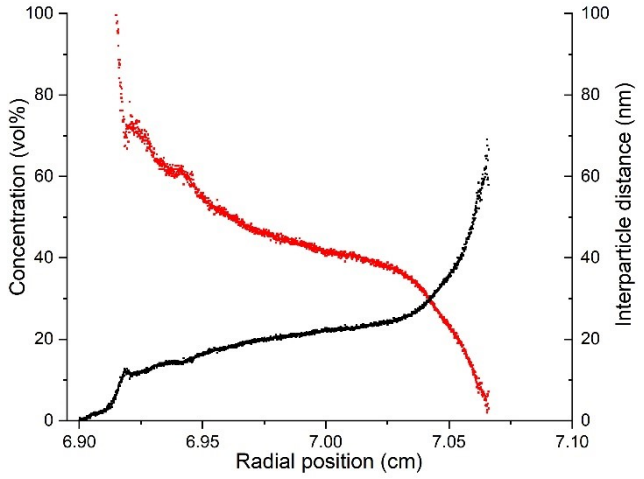

Figure S3: Experimental sedimentation-diffusion equilibrium concentration profile (black line) of 15 vol% SNPs at 1100 rpm and the conversion[14] of the volume concentration to interparticle distance (red line) by the equation $d = 2r[(\varphi_m/\varphi)^{1/3} - 1]$, where d is the interparticle distance, r the particle radius, and φ and φ_m the volume concentration and the maximum volume concentration, respectively.

SI 2: The derivation of equations for the SD profile

A macroscopic electric field was shown[9,11] to exist, which stems from the huge mass difference between the colloidal particles and the counter-ions[12]. The internal electric field E exerts a force on the colloids, which is balanced by the osmotic pressure gradient. Thus, thermodynamic equilibrium for colloids with the inclusion of a centrifugal force can be described by equation (S1):

$$-kT(d\rho/dr) - ze\rho E - m\rho\omega^2 r = 0 \quad (S1)$$

With macroscopic charge neutrality, the final equation for SD profile can be derived, as shown in equation (S2):

$$\ln(y) + z\sinh^{-1}(y) = -\left(r^2/2L_\omega^2\right) + const \quad (S2)$$

where kT is the thermal energy, r the position indicating the radial distance from the center of rotation, e the electron charge, ρ the number density of colloids, z the particle surface charge number, m the particle mass, ω the angular velocity of the centrifugation, $y = z\rho/2c_s$ the non-dimensional number density of colloids, L_ω the gravitational length. In the low-concentration region ($y << z^{-1}$), equation (S2) becomes asymptotic to a barometric exponential increase, as shown in equation (S3),

$$\rho(r) = \rho(r_1)exp\left((r^2 - {r_1}^2)/2L_\omega^2\right) \quad (S3)$$

In the intermediate-concentration region ($z^{-1} << y << 1$), equation (S2) asymptotes to a quadratic increase, as shown in equation (S4):

$$\rho(r) = \rho(r_2) + \left((r^2 - {r_2}^2)/(z^2L_\omega^2/c_s)\right) \quad (S4)$$

Finally, in the relatively high concentration region ($y >> 1$), a barometric exponential increase with an inflated gravitational length, as shown in equation (S5) should apply under the assumption of no interparticle interaction:

$$\rho(r) = \rho(r_3)exp\left((r^2 - {r_3}^2)/2(z+1)L_\omega^2\right) \quad (S5)$$

However, at the high-concentration region the interparticle interaction among like-charged SNPs needs to be considered. This can be taken into account by employing the second virial coefficient B_2[13,14], thus modifying equation (S5) significantly. Haschemeyer and Bowers[13] demonstrated that B_2 can be included in the exponents by employing the activity coefficient f, as the following: The activity a is defined as $a = cf$ where c is the concentration and f the activity coefficient. For the nonideal condition, the equilibrium distribution is given[15] by:

$$a(r) = a_m e^{H(r^2 - r_m^2)} \quad (S6)$$

where the subscript m denotes meniscus, H is defined as $H \equiv M(1 - \mathrm{K}\nabla\rho_s)\omega^2/2RT$ with ∇ the partial specific volume and ρ_s the solution density. Replacing a by cf yields:

$$c(r)f(r) = c_m f(r_m)e^{H(r^2 - r_m^2)} \quad (S7)$$

and as $f = e^{B_2 Mc}$, the final equation becomes:

$$c(r) = c_m e^{M(A\left(r^2 - r_m^2\right) - B_2(c(r) - c_m))} \quad (S8)$$

Due to the presence of *region I* and *II*, an offset constant E is added, leading to:

$$c(r) = c_m e^{M\left(A\left(r^2 - r_m^2\right) - B_2\left(c(r) - c_m\right)\right)} + E \qquad \text{(S9)}$$

and where $A = H/M$. Finally, equation (S9) can be rewritten to equation (3) after *H* is substituted by its definition.

SI 3: The inclusion of a third order virial coefficient

It might also be argued that using only a second virial coefficient (B_2) cannot describe the interactions properly. To verify whether adding a third virial coefficient (B_3) improves the fit, we excluded and included B_3 to compare the fit results, as shown in **Figure S4**. The fit value for B_3 obtained is 1.4×10^{-10} mol/(kg·vol%^{2}) (B_3M = 4.1×10^{-44} m^6). An F-test was conducted to check whether adding B_3 is statistically necessary: at a significance level of 5%, the F-value must be smaller than 0.89 to make adding B_3 significant. The F-value can be calculated as the ratio of the two adjusted R-Square values in the two fits as shown in **Figure S4**: 0.99567/0.99594 = 0.9997 > 0.89. Thus, B_3 does not significantly improve the fit and we can omit higher order virial coefficients in our case. Qualitatively speaking, silica nanoparticles are so much larger than molecules that their number density is still low, although their volume fraction is high. Therefore, a higher order virial coefficient is not needed.

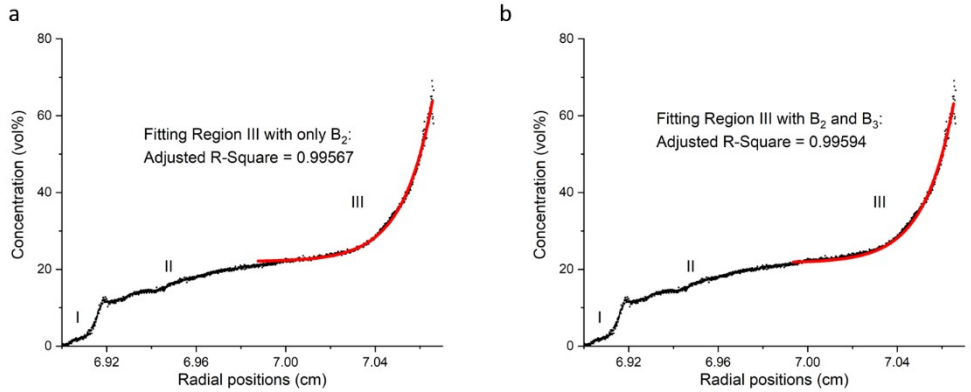

Figure S4: Fit results of region III by the inclusion of a) only B_2 and b) both B_2 and B_3. B_3 can be further considered by including the term B_3MC^2. Adding B_3 results in B_3 = 1.4×10^{-10} mol/(kg·vol%^{2}) and B_3M = 4.1×10^{-44} m^6.

SI 4: pH gradient measurement and calibration

McCrumb indicator[17] is a universal pH indicator which changes color from red to brownish and then to violet with pH value increase. Therefore, the absorbance spectrum can be used to detect a pH value change along the concentration gradient of the silica nanoparticles. A series of calibrations was firstly done with dispersions of known pH values. As it is shown in **Figure S5a**, the absorbance at 430 nm was used to characterize the pH change in our system (the absorbance peak at 650 nm overlaps with the fluorescence absorption peaks, which may induce errors). The relation between the absorbance and pH value was fitted as linear, shown in **Figure S5b**. Therefore, the absorbance difference at 430 nm before and after the addition of a tiny amount (ca. 1 μL) of McCrumb indicator (**Figure S6**) can be converted to pH values. By this means, **Figure 3b** was plotted.

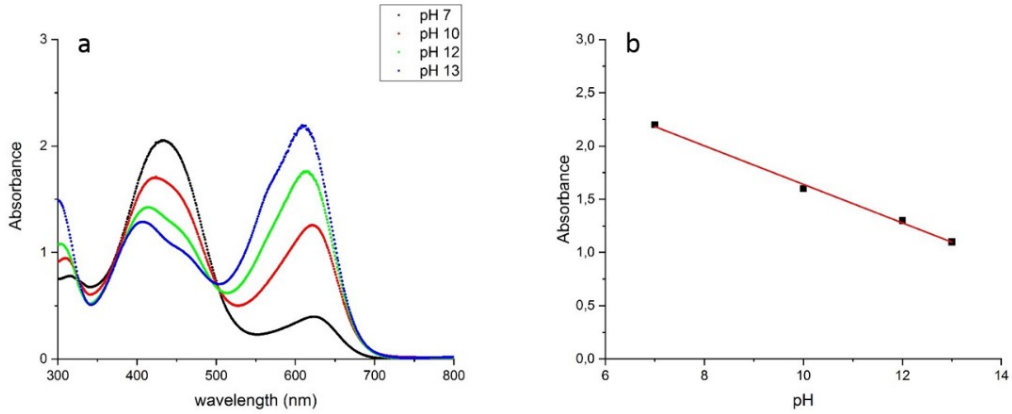

Figure S5: a) The absorbance spectrum of the home-made McCrumb indicator in dispersions of different known pH values; b) The absorbance *A* at 430 nm at different pH values (black dots) and the plots follow a linear fitting curve (red): A = 3.4 – 0.2 pH from pH 7 to pH 13.

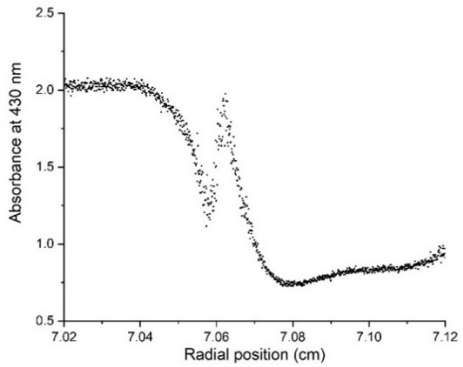

Figure S6: The absorbance gradient (at 430 nm) along the radius, characterized by pH indicator at the sedimentation-diffusion equilibrium for SNPs of an initial concentration of 15 vol% at 5000 rpm. The spike at the radius of ca. 7.06 cm is due to the phase boundary, similar as shown in **Figure 2a**.

SI 5: Detailed calculation of electric field strength from Donnan effect and pH gradient

The electric field can be estimated from the Donnan potential by using the equation[18]: $E = -m\omega^2 r/(1+z)e$, where m is the particle molecular mass (3×10^5 kg mol^{-1}), ω is the angular velocity (523 rad s^{-1}, 5000 rpm), r is the average radial position in *region III* (7 cm) and z is the particle surface charge number (49). The electric field E can be thus calculated as ca. **10 V cm^{-1}**. The electric field can be also estimated by the pH jump. The pH value close to the sediment was ca. 13, while in the meniscus part the pH was about 7. Therefore, the ion concentration jump is 10^6. The electric field can be calculated using the Nernst equation $E = (kT/e)\ln(c/c_0)$, where c is the concentration of ions close to the sediment and c_0 is the initial ion concentration near the meniscus. This leads to $\boldsymbol{E \cong 7}$ **V cm^{-1}** (with as distance from the meniscus to *region III* ca. 0.06 cm). These two values agree reasonably well, and we conclude that such a steep pH gradient resulted from the Donnan effect.

SI 6: Detailed calculation of hydroxide group density

When the concentration gradient reached the plateau value (ca. 20 vol%) in *region III* as shown in **Figure S7** (radial: 7.09 cm to 7.11 cm), the pH value reached 13 (as shown in **Figure 2b**). Since the diameter of SNPs is ca. 90 nm, the volume concentration (20 vol%) can be converted to the mole fraction ($9\cdot10^{-7}$ mol l^{-1}). As the dissociation constant for the water-glycerol mixture[19] is about 14, the concentration of surface hydroxide groups (deprotonated) can be calculated from the pH value to be $1\cdot10^{-1}$ mol l^{-1}. Therefore, the number of hydroxide groups (deprotonated) can be estimated to be 4.4 per nm^2. From the literature[20], the surface silanol group concentration is 4.9 OH groups nm^{-2}. Therefore, it means that due to the Donnan potential, 90% of silanol groups are deprotonated. At a higher radius of 7.12 cm, the concentration increased above 40 vol% and the pH value was found to decrease to 12, which means 10 times fewer hydroxyl groups were deprotonated. In this sense, the counter-ion bridge at super crowding environment agrees.

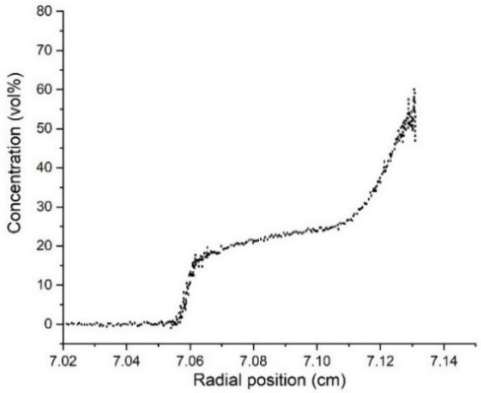

Figure S7: Experimental sedimentation-diffusion equilibrium concentration profile at 5000 rpm for SNPs of an initial concentration of 15 vol% at 5000 rpm.

SI 7: Calculation of the chemical potential to illustrate the driving force for the gel formation

An SEM image of the gel is shown in **Figure S11**, while **Figure S12** shows images of various stages after the AUC experiment. The sedimentation-diffusion equilibrium profile can be converted to an osmotic pressure difference $\Delta\Pi$ using **equation (S10)**[21]:

$$\Delta\Pi = \omega^2\left(\frac{\partial\rho}{\partial c}\right)_{\mu}\int_{r_m}^{r} c(r)\, r\, dr \qquad \text{(S10)}$$

where c is the mass concentration of the solute species, ω the angular velocity (equals 1100 rpm), and $\left(\frac{\partial\rho}{\partial c}\right)_\mu$ the density increment of the sample at constant chemical potential of water and salt, which was approximated using the density of the pure solvent and solid nanoparticles. By using **equation (S10)**, **Figure S8** was calculated from **Figure 2** as a typical example.

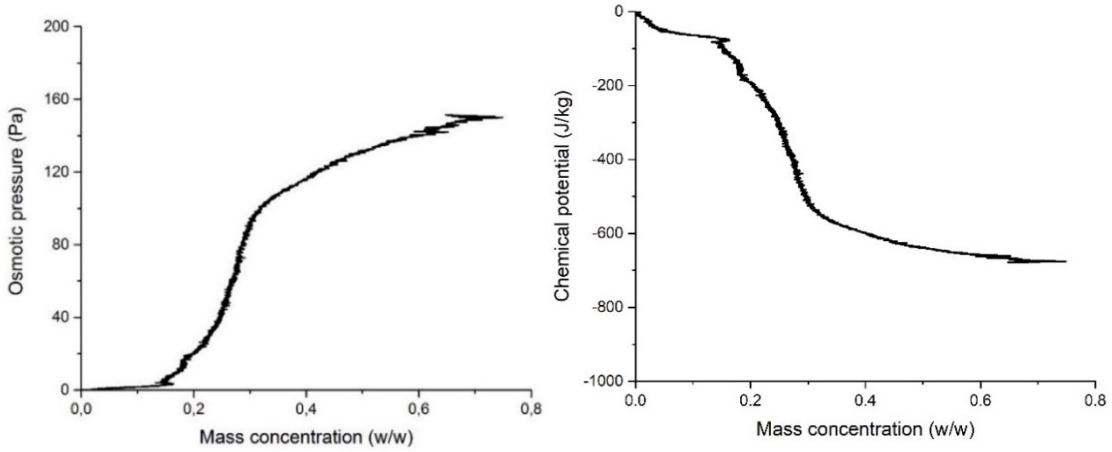

Figure S8 (left): Osmotic pressure change with mass concentration of concentrated charged silica nanoparticles, calculated from Figure 1 using equation (*3*).

Figure S9 (right): Chemical potential change with mass concentration of concentrated charged silica nanoparticles. The decrease in chemical potential with the particle concentration increase drove the gel formation at high concentration.

The solvent chemical potential difference ($\Delta\mu$) can be calculated by the generalized Svedberg-Pedersen equation[22], as shown in **equation (S11)**:

$$\Delta\mu = \omega^2 \int_{r_m}^{r} (1 - \rho v)\, r dr \tag{S11}$$

where v is the partial molar volume of the solvent and ρ is the gel density. By using **equation (S11)**, **Figure S9** was calculated.

SI 8: Residual van der Waals attraction calculation

The residual vdW attraction and the electrostatic repulsion can be estimated[23, 24] using

$$U_A = -\frac{A}{6}\left(\frac{2R^2}{(2R+H)^2 - 4R^2} + \frac{2R^2}{(2R+H)^2} + \ln\frac{(2R+H)^2 - 4R^2}{(2R+H)^2}\right) \tag{S12}$$

$$U_R = 2\pi\varepsilon_r\varepsilon_0 R\left(\frac{4kT}{ze}\tanh\left(ze\Psi_0/4kT\right)\right)^2 \ln\left[1 + exp(-\kappa H)\right] \tag{S13}$$

$$A = A_{\nu=0} + A_{\nu>0} \approx \frac{3}{4}kT\left(\frac{\varepsilon_1 - \varepsilon_2}{\varepsilon_1 + \varepsilon_2}\right)^2 + \frac{3h\nu_e}{16\sqrt{2}}\frac{(n_1^2 - n_2^2)^2}{(n_1^2 + n_2^2)^{3/2}} \tag{S14}$$

where ε_1 is the dielectric constant of solvents, ε_2 is the dielectric constant of nanoparticles, n_1 is the refractive index of solvents, n_2 is the refractive index of nanoparticles, R is the particle radius, H is the interparticle distance and A is the Hamaker constant. Furthermore, Ψ_0 is the surface potential (approximated by the zeta potential ζ), κ is the reciprocal Debye length, Z is the valency, e is the unit charge, ν_e is the so-called plasma frequency of the free electron gas, typically in the range (3–5) $\times 10^{15}$ s^{-1} and h is the Planck constant.

For a typical sample of SiO_2, the refractive index (n_2) at ca. 600 nm (the average wavelength used in AUC experiments) is 1.46. In the unlikely case that glycerol is preferably adsorbed on the surface of silica, the solvent refractive index would be n_1 = 1.47. Moreover, the effect of density inhomogeneity can be included as the vdW attraction is proportional to the density squared. If the density fluctuation $\Delta\rho$ in the silica particles is 0.2 g/cm^3 (which is already a large fluctuation) and silica has a density ρ of 1.6 g/cm^3, the relative contribution of the fluctuations to the residual vdW force is about 26%. By considering these two effects, $U_A + U_R$ can be calculated, as shown in **Figure S10**. The repulsion force dominates when the interparticle distance is larger than 1 nm, amounts to about 7kT at 5 nm and the total interparticle interaction is not attractive until the interparticle distance decreases below 0.2 nm. Therefore, the residual vdW attraction is unlikely to be the major contribution to the long-distance attraction in our findings, even if both the density fluctuation and refractive index change are considered.

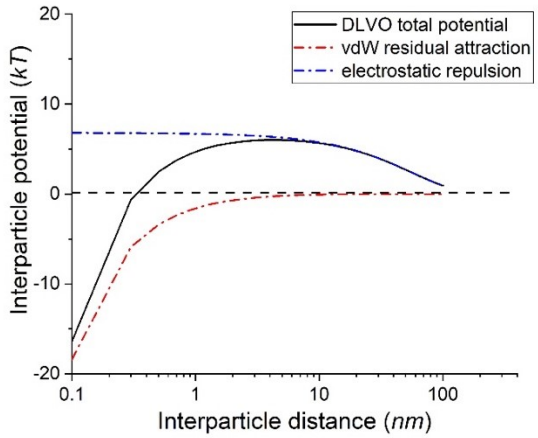

Figure S10: Interparticle potential versus interparticle distance. Plotted are the vdW attraction, due to supposed density inhomogeneity and refractive index change due to glycerol adsorption, and regular electrostatic repulsion, leading to a total barrier height of about 7*kT*.

Figure S11: The gel after the overnight immersion in salt solution (0.1 M NaCl or 0.1 M $CaCl_2$ in water), as shown in the left vessel, stayed intact. In comparison, the gel after the overnight immersion in pure water, as shown in the right vessel, dissolved into pieces.

SI 9: Background discussion on counter-ion mediated attraction

Counter-ion mediated attraction was first proposed by Sogami and Ise[25]. They attributed this attraction[26] to the difference between the electrostatic Helmholtz energy and electrostatic Gibbs energy as calculated using DLVO theory[27]. While in their approach the Helmholtz energy is always repulsive, the Gibbs energy appeared to be attractive for a certain range of conditions. However, Overbeek[28] totally disagreed, indicating that in a proper description of the DLVO theory the result obtained is already the Gibbs energy and thus does not have to be corrected. As far as we know, the debate was not settled after over 40 years[29,30]. At the same time, several experiments[31,32] indicated the existence of attraction between like-charge colloids, which cannot be explained by the DLVO theory. Thereafter, also several theories[33–36] were proposed, which all considered the vital role of counter-ions in mediating the like-charge attraction.

The classic counter-ion condensation theory[37] requires: $\zeta \geq Z^{-1}$ with $\zeta = l_B/b$ where l_B is the Bjerrum length, b is the charge site spacing and Z is the counterion valence. In our case, l_B = 14 nm and Z = 1. The typical OH group density on silica[38] equals 5 per nm^2, so the site spacing is ca. 0.44 nm if square packing is assumed. Therefore, ζ / Z = ca. 32 >>1 and the counter-ion mediated force is likely.

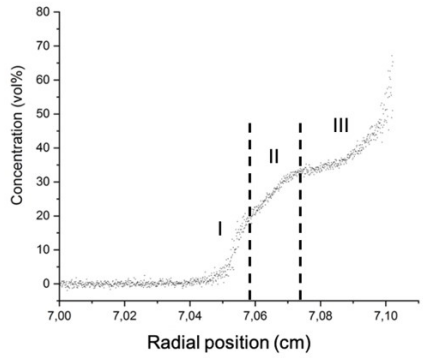

Figure S12: Experimental sedimentation-diffusion equilibrium profiles (three-region) for a concentrated charged SNP at an initial concentration of 10 vol% of a different batch of silica nanoparticles with the average diameter of 140 nm.

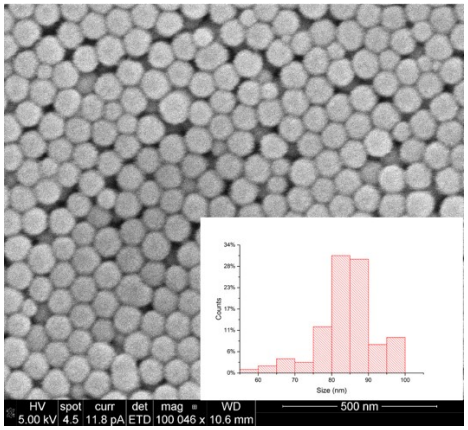

Figure S13: The size distribution of the synthesized silica nanoparticles, characterized by SEM. More than 100 particles were counted and the average particle diameter is 84 nm ± 8 nm.

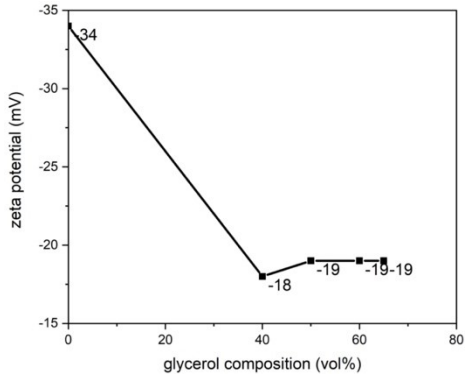

Figure S14: The evolution of zeta potential of silica nanoparticle dispersion as a function of glycerol composition. Measuring above 65% appeared to be impossible because the signal became extremely weak due to nearly refractive index matching. Data for less than 40 vol% glycerol are not measured as the value at 80 vol% is required which is therefore estimated using the data for 40 to 65 vol%.

References

1. X. Xu, T. Franke, K. Schilling, N. A. J. M. Sommerdijk, H. Cölfen, *Nano Letters* **19**, 1136-1142 (2019)
2. T. G. Souza, V. S. Ciminelli, N. D. S. Mohallem, in *Journal of Physics: Conference Series*. (IOP Publishing, 2016), vol. 733, pp. 012039.
3. J. Tuoriniemi, A.-C. J. Johnsson, J. P. Holmberg, S. Gustafsson, J. A. Gallego-Urrea, E. Olsson, J. B. Pettersson, M. Hassellöv, *Science and Technology of Advanced Materials* **15**, 035009 (2014).
4. P. Eaton, P. Quaresma, C. Soares, C. Neves, M. De Almeida, E. Pereira, P. West, *Ultramicroscopy* **182**, 179-190 (2017).
5. R. Amini, S. K. Brar, M. Cledon, R. Y. Surampalli, *Journal of Hazardous, Toxic, and Radioactive Waste* **20**, B4015004 (2016).
6. A. Bootz, V. Vogel, D. Schubert, J. Kreuter, *European Journal of Pharmaceutics and Biopharmaceutics* **57**, 369-375 (2004).
7. E. Karabudak, H. Cölfen, in *Analytical Ultracentrifugation: Instrumentation, Software, and Applications,* A. F. Uchiyama S., WE. Stafford, T. Laue, Eds. (Springer, Tokyo, 2016).

8. J. Pearson, J. Walter, W. Peukert, H. Cölfen, *Analytical Chemistry* **90**, 1280-1291 (2018).
9. M. Rasa, B. Erné, B. Zoetekouw, R. van Roij, A. Philipse, *Journal of Physics: Condensed Matter* **17**, 2293-2314 (2005).
10. I. Nieduszynski, Dynamic properties of biomolecular assemblies, S.E. Harding and A.J. Rowe, eds. (Elsevier, 1990).
11. P. Schuck, *Biophysical Journal* **78**, 1606-1619 (2000).
12. K. Osseo-Asare, F. Arriagada, *Colloids and Surfaces* **50**, 321-339 (1990).
13. H. Giesche, *Journal of the European Ceramic Society* **14**, 189-204 (1994).
14. T. Hao, R. E. Riman, *Journal of Colloid and Interface Science* **297**, 374-377 (2006).
15. R. H. Haschemeyer, W. F. Bowers, *Biochemistry* **9**, 435-445 (1970).
16. A. Philipse, A. Vrij, *Journal of Physics: Condensed Matter* **23**, 194106 (2011).
17. F. McCrumb, *Industrial & Engineering Chemistry Analytical Edition* **3**, 233-235 (1931).
18. A. P. Philipse, *Journal of Physics: Condensed Matter* **16**, S4051-S4062 (2004).
19. D. D. Perrin, *Dissociation Constants of Organic Bases in Aqueous Solution: supplement 1972*, Butterworths, 1972.
20. L. Zhuravlev, *Langmuir* **3**, 316-318 (1987).
21. A. Brian, H. Frisch, L. Lerman, *Biopolymers: Original Research on Biomolecules* **20**, 1305-1328 (1981).
22. H. Cölfen, *Biotechnology and Genetic Engineering Reviews* **16**, 87-140 (1999).
23. G. de With, Chapter 7 in *Polymer Coatings,* (Wiley-VCH Verlag GmbH, Weinheim, 2018).
24. J. N. Israelachvili, *Intermolecular and Surface Forces* (Academic Press, 2015).
25. I. Sogami, N. Ise, On the Electrostatic Interaction in Macroionic Solutions. *The Journal of Chemical Physics* **1984**, *81* (12), 6320–6332.
26. N. Ise, When, Why, and How Does like like Like? *Proceedings of the Japan Academy, Series B* **2007**, *83* (7), 192–198.
27. B. Derjaguin, L. Landau, Theory of the Stability of Strongly Charged Lyophobic Sols and of the Adhesion of Strongly ChargedParticles in Solutions of Electrolytes, *Progress in Surface Science* **1993**, *43* (1–4), 30–59.
28. J.T.G. Overbeek, On the Electrostatic Interaction in Macroionic Solutions and Suspensions. *The Journal of Chemical Physics* **1987**, *87* (8), 4406–4408.
29. Y. Levin, When Do like Charges Attract? *Physica A: Statistical Mechanics and its Applications* **1999**, *265* (3–4), 432–439.
30. Y. Levin, Electrostatic Correlations: From Plasma to Biology, *Reports on Progress in Physics* **2002**, *65* (11), 1577.
31. K. Ito, H. Yoshida, N. Ise, Void Structure in Colloidal Dispersions, *Science* **1994**, *263* (5143), 66–68.
32. A.E. Larsen, D.G. Grier, Like-Charge Attractions in Metastable Colloidal Crystallites, *Nature* **1997**, *385* (6613), 230–233.
33. P. Linse, V. Lobaskin, Electrostatic Attraction and Phase Separation in Solutions of Like-Charged Colloidal Particles, *Physical Review letters* **1999**, *83* (20), 4208.
34. P. Linse, V. Lobaskin, Electrostatic Attraction and Phase Separation in Solutions of Like-Charged Colloidal Particles, *The Journal of Chemical Physics* **2000**, *112* (8), 3917–3927.
35. I. Rouzina, V.A. Bloomfield, Macroion Attraction due to Electrostatic Correlation between Screening Counterions, 1. Mobile Surface-Adsorbed Ions and Diffuse Ion Cloud. *The Journal of Physical Chemistry* **1996**, *100* (23), 9977–9989.
36. E. Allahyarov, I. D'Amico, H. Löwen, Attraction between Like-Charged Macroions by Coulomb Depletion, *Physical Review Letters* **1998**, *81* (6), 1334.
37. S. Pietronave, L. Arcesi, C. D'Arrigo, A. Perico, Attraction between Like-Charged Polyelectrolytes in the Extended Condensation Theory, *The Journal of Physical Chemistry B* 112, 15991-15998 (2008).
38. R. K. Iler, The Chemistry of Silica: Solubility, Polymerization, Colloid and Surface Properties and Biochemistry of Silica, Wiley (New York, 1979).